A High Performance Lithium-Sulfur Battery Enabled by Fish-Scale Porous Carbon/Sulfur Composite and Symmetric Fluorinated Diethoxyethane Electrolyte

Mengyao Gao[a, d], ChiCheung Su[a], Meinan He[a], Tobias Glossmann[b], Andreas Hintennach[c], Zhenxing Feng[a], Yaqin Huang[d], Zhengcheng Zhang[a,*]

[a]*Chemical Sciences and Engineering Division, Argonne National Laboratory, 9700 S. Cass Avenue, Argonne, IL 60439, USA*

[b]*Mercedes-Benz Research & Development North America, Inc., 12120 Telegraph Road, Redford, MI 48239, USA*

[c]*Daimler AG (Mercedes-Benz Cars), Group Research, HPC G012-BB, 71034 Boeblingen, Germany*

[d]*State Key Laboratory of Chemical Resource Engineering, Beijing Laboratory of Biomedical Materials, Beijing University of Chemical Technology, 15 Beisanhuan East Road, Beijing, 100029, China.*

Email: zzhang@anl.gov, 1-630-252-7868

Abstract

A high performance lithium-sulfur (Li-S) battery comprising of a symmetric fluorinated diethoxyethane electrolyte coupled with a fish-scale porous carbon/S composite electrode was demonstrated. 1,2-Bis(1,1,2,2-tetrafluoroethoxy) ethane (TFEE) was first studied as a new electrolyte solvent for Li-S chemistry. When co-mixed with DOL, the DOL/TFEE electrolyte suppressed the polysulfide dissolution and shuttling reaction. When coupled with a fish-scale porous carbon/S composite electrode, the Li-S cell exhibited a significantly high capacity retention of 99.5% per cycle for 100 cycles, which is far superior to the reported numerous systems.

KEYWORDS: lithium-sulfur battery; fluorinated electrolyte; 1,2-bis(1,1,2,2-tetrafluoroethoxy) ethane; fish-scale porous carbon/sulfur composite; suppression of lithium polysulfide dissolution

1. Introduction

The nascent lithium-ion batteries have dominated battery market for portable electronics since their launch in the early 1990s. It is believed to be promising candidates for electric vehicles and electrical grid applications. However, these batteries cannot offer a suitably long driving range (i.e., >300 km) for pure electric vehicles due to their limited energy density of about 200-250 $Whkg^{-1}$ at present.[1-3] The lithium-sulfur battery (LiSB) is a promising next-generation battery generation technology, and it has potential to meet the performance requirements for high-energy-density batteries in emerging electronics and vehicle applications.[4-9] Sulfur is a naturally abundant and nontoxic element, and one of the cheapest energy storage materials with an extremely high specific capacity of 1675 $mAhg^{-1}$.[10-12] During the discharge-charge, sulfur is electrochemically reduced to lithium polysulfides (LiPS) intermediates through a multistep process, where the longer chain LiPS tends to dissolve in the electrolyte causing severe redox shuttling reaction and poor Coulombic efficiency.[13-17] Insoluble discharge products such as Li_2S_2 and Li_2S are generated at the final step. During the charging step, Li_2S/Li_2S_2 is converted to elemental sulfur through the multiple oxidation steps. Inspired by nature, Huang's group[23, 24, 48] fabricated the hierarchical fish-scale porous carbon (FSPC) as substrate for sulfur cathode. Although the performance LSB using the FSPC/Sulfur composite electrode was improved, the dissolution of the intermediate lithium polysulfides (LiPS) during cycling and its subsequent issues such as redox shuttling, low Coulombic efficiency and fast capacity fade still remains unsolved.[6,7,18]

A firm understanding of the operation mechanism and the technical solution to solve the aforementioned issues are in great demand to successfully develop commercial LiSB.[19,20] Extensive approaches have been undertaken to overcome these problems: i) to introduce porous

carbon materials into the cathode for trapping LiPS within the cathode during cycling by the strong adsorption property of carbon;[21-27] ii) to form a protective layer on the anode surface to mitigate the redox reaction of the dissolved LiPS and lithium metal;[28,29] and iii) to develop new solid-state electrolyte,[30,31] electrolytes consisting of ionic liquid,[32-34] tetra (ethylene glycol) dimethyl ether[35,36] as organic solvents for the electrolyte, lithium salt electrolytes,[37,38] and functional electrolyte/additives[39,40] for preventing the dissolution of the LiPS into the electrolyte and thereby avoid the redox shuttling effect.

Hydrofluoroethers could suppress the dissolution of lithium polysulfides into the electrolyte, therefore mitigate the shuttling effect with improved Coulombic efficiency and capacity retention.[41-46] In our previous papers, a single fluorinated ether 1,1,2,2-tetrafluoroethyl-2,2,3,3-tetrafluoropropyl ether (TTE) was reported as an efficient electrolyte co-solvent for LiSB.[45,46]

In this paper, we report a new LiSB chemistry coupling a diether-based fluorinated compound, 1,2-bis (1,1,2,2-tetrafluoroethoxy) ethane (TFEE), as a new electrolyte co-solvent with a fish-scale porous carbon/sulfur composite electrode. The fabulous cell performance demonstrated in the LiSB suggests the combination of a fluorinated electrolyte with a sulfur cathode with hierarchical porous carbon provides a solution to the problems plagued the LiSB technology.

2. Experimental

2.1 Preparation of Materials

The detailed preparation of the fish scale porous carbon was described in reference 23 and 24. The fish scales from grass carp (Ctenopharyn Odon Idellus) were pre-carbonized at 330^{o}C for 2 h in a muffle furnace, which were then treated with KOH aqueous solution for activation. The carbon

material was obtained after subject to a heating protocol under N_2 in a tubular furnace: 1) ramp at 3°C min^{-1} to 400°C and held for 30 min, and 2) increase temperature to 900°C and kept for 1 h. After cooling down to the room temperature, it was diluted by HNO_3 and rinsed by distilled water, then dried at 120°C for 12 h. The surface area of the as-prepared porous carbon is 2732 m^2g^{-1}, the micropore volume is 0.706 cm^3g^{-1} and the total volume is 1.69 cm^3g^{-1}.

2.2 Sulfur Cathode Fabrication

Sulfur (99.8%, analytical grade, Sigma-Aldrich), fish-scale porous carbon, carbon black and PVDF binder (5 wt% in NMP solution) were mixed with weight ratio of 42%, 28%, 20% and 10%, respectively. The slurry was then coated onto an aluminum foil current collector. N-Methyl-2-pyrrolidone (NMP) was used to dissolve the PVDF binder and adjust the slurry viscosity. The coated electrodes were dried at 60 °C under vacuum for 12 h and punched into discs with an area of 1.27 cm^2 with a sulfur loading of 2 $mgcm^{-2}$. The detailed preparation and properties of the sulfur composite electrode has been reported in previous papers.[23,24]

2.3 Preparation of Electrolyte

1,2-Bis(1,1,2,2-tetrafluoroethoxy) ethane (TFEE) was purchased from Synquest Labs, which was subject to a vacuum distillation for purification. Its purity was determined by GC-MS and its structure was analyzed by NMR spectroscopy. 1,2-Dimethoxyethane (DME), 1,3-dioxolane (DOL), lithium bis(trifluoromethanesulfonyl)imide (LiTFSI) and sublimed sulfur were purchased from Sigma-Aldrich. All solvents were purified by regular distillation before use. DOL/DME and DOL/TFEE mixture solvents and electrolyte preparation were performed in an Ar-filled glove-box with controlled moisture content < 1 ppm. The electrolytes studied were (1) a baseline electrolyte of 1.0 M LiTFSI/DOL/DME (5/5 by volume) and (2) 1.0 M LiTFSI in DOL/TFEE with various

volume ratios (8/2, 7/3, 5/5, 3/7 and 2/8). NMR spectra were acquired on a 300 MHz Bruker spectrometer. ^{1}H chemical shifts were referenced to chloroform-*d* at 7.27 ppm and ^{19}F chemical shifts were referenced to $CFCl_3$. NMR spectra are shown in Figure S1 in Supplemental Information.

2.4 Evaluation of Electrochemical Properties

2032 coin cells were assembled with lithium as the anode, the above sulfur electrode as cathode, Celgard 2325 as separator and 30 μL electrolyte. The cells were assembled in an Ar-filled glove-box and cycled with C/10 (1C=1675 mAg^{-1}) current on a Maccor series 4000 cycler with a 1.6-2.8 V voltage range. The charging process was terminated by a cut-off voltage of 2.8 V for all the DOL/TFEE electrolyte cells.

2.5 Examination of Electrode Morphology

For morphological analysis of electrodes, the samples were loaded onto an air-tight scanning electron microscopy (SEM) sample holder. The high resolution scanning electron microscope (JEOL JSM6610) was operated at 5-10 kV for imaging and 10-20 keV for energy-dispersive X-ray spectroscopy (EDS) data.

3. Results and Discussion

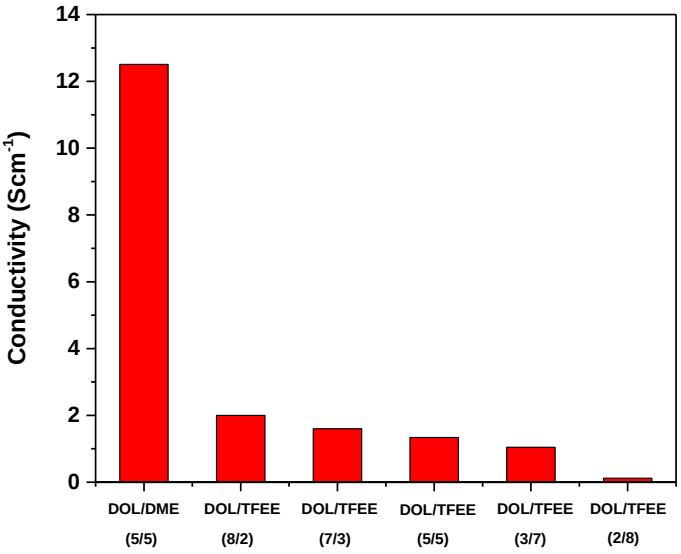

Figure 1. Conductivity of DOL/TFEE electrolytes with 1.0 M LiTFSI at 25 ^{o}C.

3.1 Electrode Material and Fluorinated Electrolyte.

A hierarchical porous carbon obtained from fish scales[23-24] has been employed to design and prepare a novel porous nanocomposite of sulfur/carbon. In this structure, the embedded sulfur is located in micropores in a highly dispersed state through capillary action. The high specific surface area of the micropores significantly improves its reactivity and reduces the loss of active materials. In addition, the void in the nanocomposite can accommodate the volume expansion of sulfur generated during the electrochemical reaction, reduce lithium polysulfide dissolution, and tremendously alleviate the shuttle effect. A symmetric fluorinated diethoxyethane was used as co-solvent for electrolyte. Five fluorinated electrolytes were prepared in the Argon-filled glove-box with 1.0 M LiTFSI dissolved in various volume ratios (8/2, 7/3, 5/5, 3/7, and 2/8) of DOL and TFEE mixture solvent. The effect of TFEE addition on the electrolyte conductivity was studied. Figure 1 shows the room temperature conductivity measured by electrochemical impedance

spectroscopy (EIS) using a coin cell fixture. Compared with DOL/DME baseline electrolyte, the conductivity of the fluorinated electrolytes DOL/TFEE is one magnitude lower and decreases gradually with the increasing amount of TFEE co-solvent. Fluorination plays a significant role in Li^+ ion solvation and kinetics of the ion transfer. Cheng *et al.*[46] recently reported that the solvation energy of fluorinated ethers is much lower than their non-fluorinated counterparts, indicating that Li^+ ions energetically favor the chelation with non-fluorinated solvent DOL in our studied DOL/TFEE system. Although the lithium salt concentration in the five DOL/TFEE mixtures is the same, the chelating geometry and the hydrodynamic radius of the solvated clusters are altered with the ratio of the DOL to TFEE, which clearly correlates to its conductivity. For the high TFEE concentration electrolyte DOL/TFEE (2/8), the conductivity is only 0.1 $mScm^{-1}$, which is ten times lower than that of DOL/TFEE (5/5) electrolyte. Therefore, the optimal concentration of TFEE is 30-50% in the mixture to afford the fast electron transfer during battery cycling realized by the Li^+ shuttling within the electrolyte media.

3.2 Enhanced Electrochemical Performance

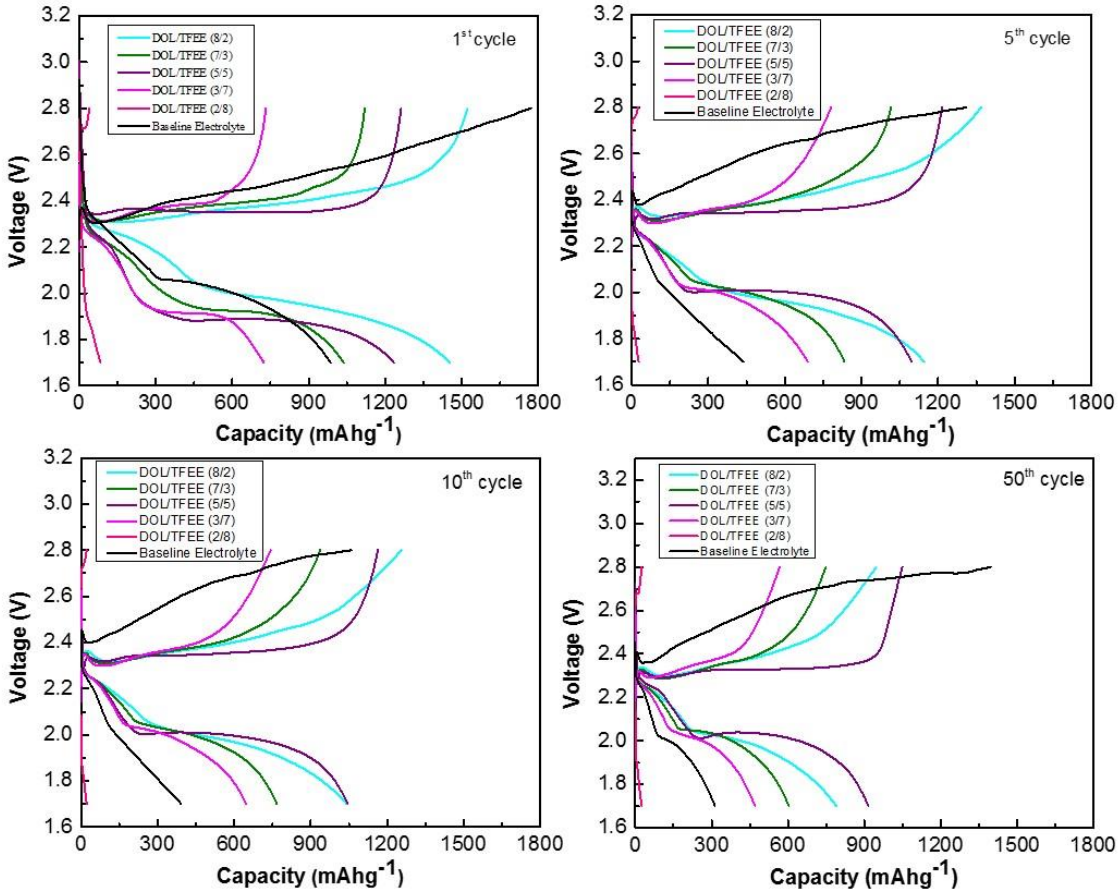

Figure 2. Voltage profiles evolution of LiSB at different cycle stages. (a) 1st, (b) 5th, (c) 10th and (d) 50th cycle. The examined electrolytes are mixtures of 1.0 M LiTFSI DOL/TFEE in various volume ratios (8/2, 7/3, 5/5, 3/7 and 2/8) with 1.0 M LiTFSI DOL/DME (5/5 by volume) was used as baseline electrolyte.

Figure 2 illustrates the charge-discharge voltage profiles of LiSB employing fluorinated electrolytes 1.0 M LiTFSI DOL/TFEE (8/2), DOLTFEE (7/3), DOL/TFEE (5/5), DOL/TFEE (3/7), DOL/TFEE (2/8) and baseline electrolyte 1.0 M LiTFSI DOL/DME (5/5) at different cycling stages. Two discharge plateaus were observed in the 1st, 5th, 10th and 50th cycle: the higher voltage plateau at 2.2-2.4 V is due to the reduction of elemental sulfur to LiPS (Li_2S_x, where $4 \leq x \leq 8$), and

the subsequent reduction to low-ordered species (Li_2S_2 and/or Li_2S) at the lower voltage plateau at 2.1-2.0 V. It is surprising that the baseline electrolyte cell showed a huge voltage polarization in the 1st charge-discharge profile and this over-potential became larger with extended cycling as shown in Figures 2c and 2d despite the highest conductivity of the electrolyte. It indicates that fluorinated electrolyte has improved wettability when in contact with the FSPC/S composite cathode and electrochemical/chemical stability to afford repeated cycling operation. While the first plateau of the LiSB with DOL/TFEE (2/8) electrolyte almost disappeared which might be caused by its low ionic conductivity (Figure 1), a significant difference in Coulombic efficiency (CE) was observed between DOL/TFEE electrolyte cells and the baseline cell.

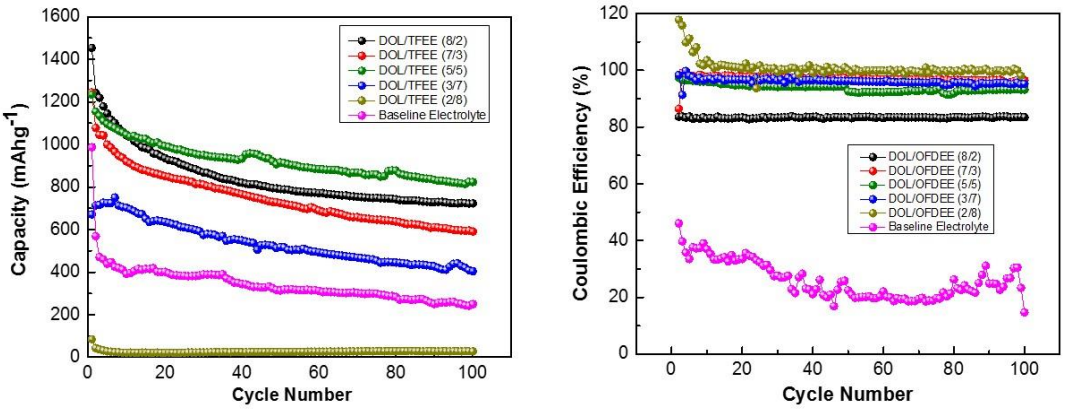

Figure 3. Cycling performance and CE of the LiSB using fluorinated electrolytes with different DOL/TFEE volume ratios 8/2, 7/3, 5/5, 3/7 and 2/8 and baseline 1.0 M LiTFSI DOL/DME (5/5) electrolyte.

Figure 3 presents the capacity retention profiles and CE as functions of cycle numbers for LiSB. Fluorinated electrolyte with 20%-70% TFEE outperformed the baseline cell, showing the highest capacity retention at 50%. 80% TFEE electrolyte failed to support the normal charge-discharge operation of the cell due to its extremely low ionic conductivity. The initial specific discharge

capacity with 20% TFEE is 1453 $mAhg^{-1}$ and 723 $mAhg^{-1}$ after 100 cycles at a rate of C/10 (1C=1675 $mAhg^{-1}$) with the CE of around 85%. After different amounts of TFEE were added to the electrolyte, both capacity and CE are improved. Interestingly, the LiSB with 50% TFEE electrolyte exhibited excellent electrochemical performance in terms of capacity retention and CE as shown Figure 3a and 3b. The initial capacity is 1234 $mAhg^{-1}$ and the capacity retention is almost 99.5% per cycle indicating the effective inhibition of the polysulfide shuttling effect in the fluorinated electrolyte. Moreover, the CE improved dramatically and remained at 97% during the cycle test. It is noteworthy that the cell performance decreases which is only slightly better than the baseline cell when the amount of TFEE further increases. It is evident that 70% and 80% TFEE leads to the low ionic conductivity (data in Figure 1), which hinders ion transport and thus leads to a low capacity retention. Further, although the difference in conductivity for DOL/TFEE (3/7) and DOL/TFEE (2/8) is quite small, the solvation sheath alters much when DOL concentration is further reduced. For DOL/TFEE (2/8), Li^+ solvation by DOL primary solvent is completely saturated, and the chance of solvation of extra Li^+ is little, meaning the discharged high order lithium polysulfides have little dissolution due to the lack of driving force in the saturated 1.0 M LiTFSI DOL/TFEE (2/8) electrolyte. As reported by many other researchers,[13,17-18] the controlled/limited dissolution of lithium polysulfides are required to facilitate the Li-S redox chemistry. This result serves as a further evidence.

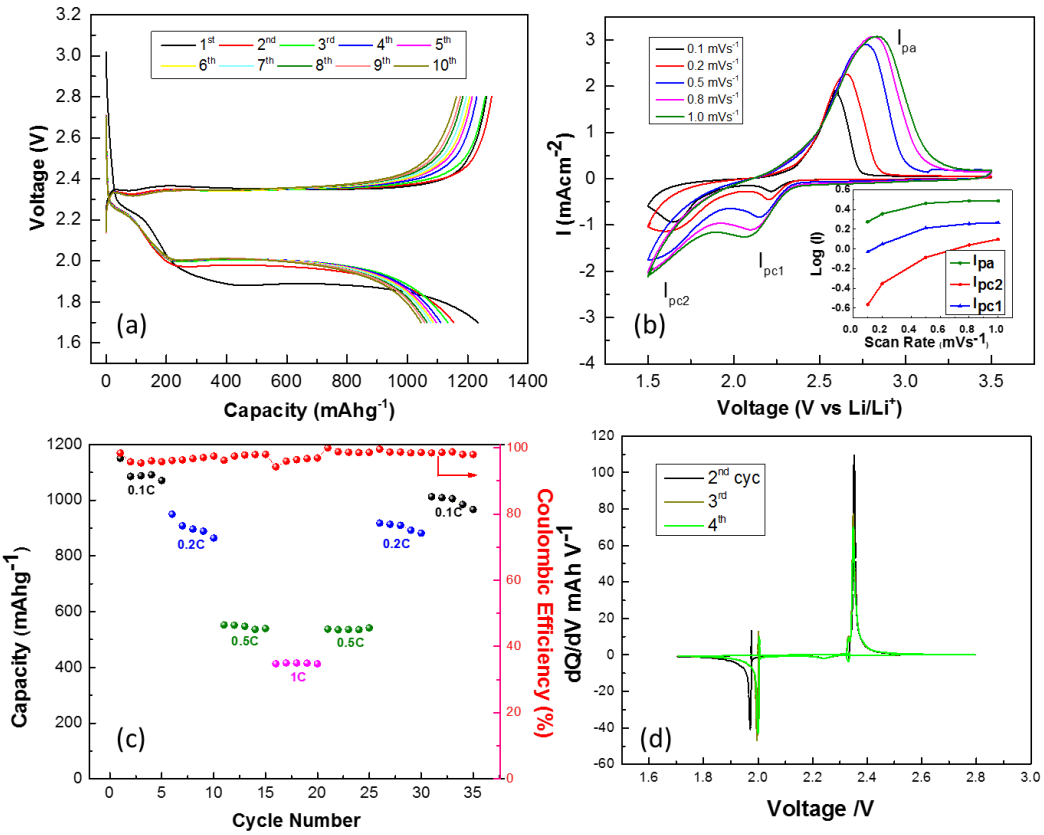

Figure 4. (a) The 1st-10th charge-discharge profiles, (b) cyclic voltammograms for LiSB employing 1.0 M LiTFSI DOL/TFEE (5/5). (the scan rate varies from 0.1, 0.2, 0.5, 0.8, to1.0 mVs^{-1}; the inset is logarithm of the peak current as a function of the potential scanning rate), (c) C-rate performance (charge at 0.1C, discharge at 0.1 C, 0.2 C, 0.5 C and 1.0 C), and (d) dQ/dV profiles of the 2nd, 3rd, and 4th cycle.

Figure 4a shows the charge-discharge voltage profiles of a LiSB employing 1.0 M LiTFSI DOL/TFEE (5/5) electrolyte at a rate of C/10 with a cutoff voltage of 2.8-1.7 V for the initial 10 cycles. The first discharge plateau corresponds to 200 $mAhg^{-1}$ and the second discharge plateau contributes 954-845 $mAhg^{-1}$ discharge capacity. In addition, the specific capacity vs. voltage profiles almost overlapped in the upper and lower discharge voltage plateaus, demonstrating that

the FSPC with the TFEE solvent really plays a role in preventing the polysulfides migrating out of the cathode from dissolving into the electrolyte.

Figure 4b shows the CV of the as-prepared DOL/TFEE (5/5) electrolyte cell with scan rates from 0.1, 0.2, 0.5, 0.8, to 1.0 mVs^{-1}. The LiPS exhibits two cathodic current peaks and one anodic current peak at the various scanning rates. The potential of the I_{pc1} exactly agrees with that observed from the reduction of elemental sulfur. In the following cathodic scanning, the high-order LiPS disproportionation into low-order LiPS and elemental sulfur which resulting in the appearance of a well distinguishable I_{pc1}. Logarithm values of the peak currents are plotted as a function of the potential scanning rate was included in the inset of Figure 4b. It is shown that all three peak currents do not follow straight linear "logI~V" relationship. This result demonstrated that the redox reactions of elemental sulfur and LiPS are not diffusion-controlled; instead it is a multi-stage redox process. Multi-scan cyclic voltammetry were also performed on the LiSB with various DOL/TFEE electrolytes at a fixed scan rate of 0.1 mVs^{-1}. The results were shown in Figure S2 in the Supplemental Information. Figure S2a is the cyclic voltammogram of 1.0 M LiTFSI in DOL/TFEE (8/2) electrolyte cell. Two cathodic peaks appear at 1.85 and 2.20 V and two anodic peaks at 2.50 and 2.63 V. The anodic peak at 2.63 V and the cathodic peak at 2.20 V correspond to the transformation between S_8 and L_2S_x ($4 \leq x \leq 8$), while the cathodic peak at 2.50 V and the anodic peak at 1.85 V to transformation between soluble polysulfides and insoluble Li_2S_2 or Li_2S. With the TFEE content increased to 50%, only one anodic peak at 2.62 V was observed during the oxidation scan (Figure S2c). This peak overlaps for all five scans indicating good reversibility in electrochemical reduction/oxidation reaction. Further increase of the TFEE content to 80% (Figure S2e) resulted in one cathodic peak loss and the potential polarization increased. However, for the baseline 1.0 M LiTFSI DOL/DME (5/5) electrolyte cell, a broad anodic reaction peak and two

broad cathodic peaks were observed in all five scans, as shown in Figure S2f. The broad peaks suggest the sluggish kinetic of the reduction and oxidation reaction of the baseline cell, leading to the dissolution of lithium polysulfides and polarization in potential. This is in good agreement with the results shown in Figure 2 in the Results and Discussion section.

The rate performance of the FSPC employing 1.0 M LiTFSI DOL/TFEE (5/5) is comparable to the state-of-the-art electrolyte. As shown in Figure 4c, at the rates of 0.1C, 0.2C, 0.5C and 1C (charged at 0.1C), the as-prepared system delivered high initial discharge capacities of 1071 $mAhg^{-1}$, 864 $mAhg^{-1}$, 539 $mAhg^{-1}$ and 413 $mAhg^{-1}$, respectively. It still kept high discharge capacities of 967 $mAhg^{-1}$, 882 $mAhg^{-1}$, and 542 $mAhg^{-1}$ with CE around 100% even after 20 cycles. The excellent electrochemical behavior of the TFEE-based fluorinated electrolyte combined with FSPC/sulfur composite cathode is confirmed by the differential capacity (dQ/dV) profiles of the galvanostatic test. As shown in Figure 4d, upon discharging, sulfur reacts with Li via a two-electron reduction process forming lithium polysulfide intermediates (Li_2S_x, x=4-8) and lithium sulfide (Li_2S) at the end of discharge at ~2.0 V. The reverse reaction occurs at around 2.4 V, leading to the conversion of Li_2S back to sulfur. A complete overlapping of the anodic and cathodic peak profiles were observed for 2^{nd}, 3^{rd}, and 4^{th} cycles as well as peak sharpness, suggesting high reversibility and fast electrode kinetics of this LiSB chemistry.

3.3 Impedance Analysis by in-situ EIS

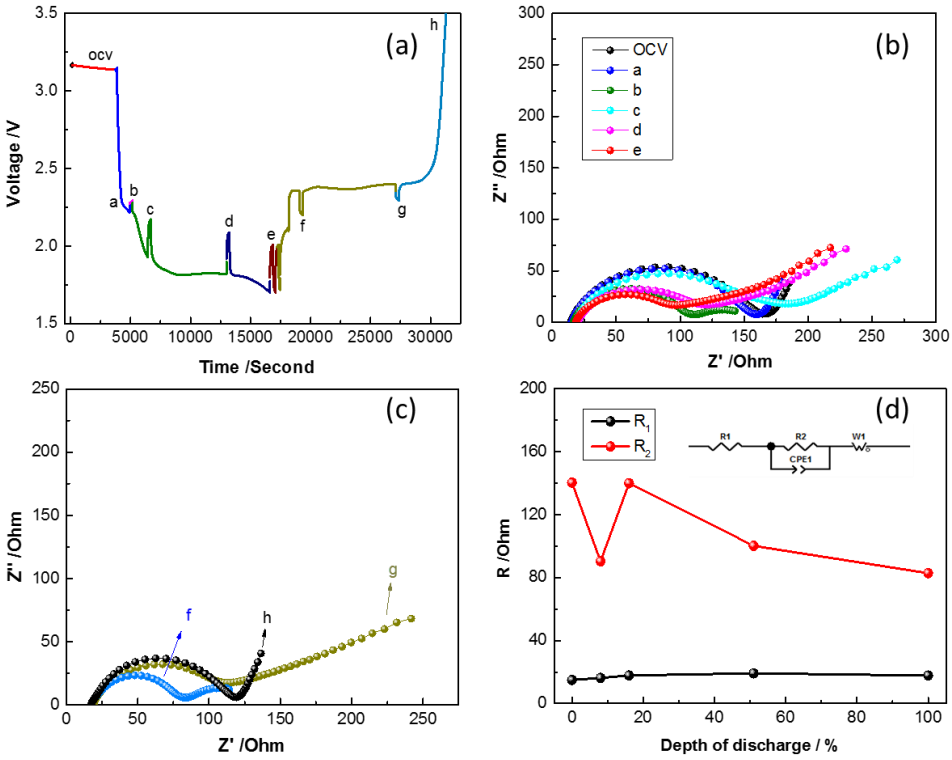

Figure 5. (a) Charge-discharge voltage profile during the *in-situ* EIS measurement, (b) recorded EIS spectra during discharge step, (c) recorded EIS spectra during charge step, and (d) resistance and impedance with depth of discharge (inset is the equivalent circuit model).

The outstanding electrochemical performance of the studied LiSB motivated us to further analyze its reaction mechanism. The impact of Depth of Discharge (DOD) and State of Charge (SOC) on the impedance was investigated *in-situ*. Figure 5a shows the 1st cycle voltage profiles and various DOD stages where the EIS is measured. Figure 5b and 5c are the Nyquist plots obtained at different DOD and SOC stages. With DOD increasing from pristine (a), 8% (b), 16% (c), 85% (d) to 100% (e), the impedance derived from the medium frequency semi-circle generally decreases in trend. During the charging process, the impedance is gradually increased with SOC as shown in Figure 5c.

To better understand the electrode/electrolyte interface, Nyquist plots from Figures 5b and 5c were analyzed using an equivalent circuit model proposed as an inset in Figure 5d. R_1 is the cell resistance and R_2//CPE_1 is the charge transfer resistance and its related capacitance. W_1 is diffusion impedance representing the Li^+ diffusion process. R_1, R_2 and CPE_1were determined by the curve fitting using Zview software (Solartron) with the equivalent circuit. Table S1 summarized the DOD dependence of the R_1, R_2, and CPE_1. During the discharge and charge process, R_1 remains stable (Figure 5d). R_2 decreases first from 140.30 Ω to 90.36 Ω, and then increases to 140.00 Ω, during initial discharge, and decreases with the following discharge at the second plateau, indicating that the TFEE-based electrolyte could stabilize the electrode/electrolyte interface by the formation of a protective film on the electrode surface.

3.4 Inhibition of LiPS Dissolution

The above electrochemical analysis confirms fluorinated electrolyte suppressed the lithium polysulfide dissolution thus prevent the deleterious redox shuttling effect of the Li-S cell. This effect also reflected by the quite different electrode morphology. Figures 6 and 7 present the SEM images of the sulfur electrode discharged in 1.0 M LiTFSI DOL/DME (5/5) and 1.0 M LiTFSI DOL/TFEE (5/5) electrolyte at different DOD stages. For the DOL/DME 1.0 M LiTFSI cycled cell, the morphology changes with the DOD and significant deposition of the discharged products on the surface of the electrode were observed at the end of the discharge as shown in Figure 6f. In contrast, the sulfur electrode discharged in DOL/TFEE electrolyte didn't show big difference as discharge proceeds from Figure 7b, 7c to 7d and only trivial deposits showed up at the very end of the discharge as shown in Figure 7. Fluorinated ether electrolytes enabled the redox reaction within the porous structure and promoted the repeated conversion of the sulfur chemistry affording a long

term cyclability of the Li-S cell. From this study, it is also manifest that the new design of the sulfur electrode could not be sufficient enough for a stable Li-S battery, nevertheless the combination of an architected electrode coupled with a fluorinated electrolyte provides a solution to the stable Li-S battery chemistry. Figure S3 in Supplemental Information illustrated pictures of the harvested electrolytes diluted with DOL solvent. Clearly, the colorless solution for the harvested DOL/TFSS electrolyte was observed at each DOD stages compared with the DOL/DME electrolyte, indicating LiPS was significantly suppressed. Electrode morphology evolution with cycling was shown in Figure S4 and Figure S5 in the Supplemental Information.

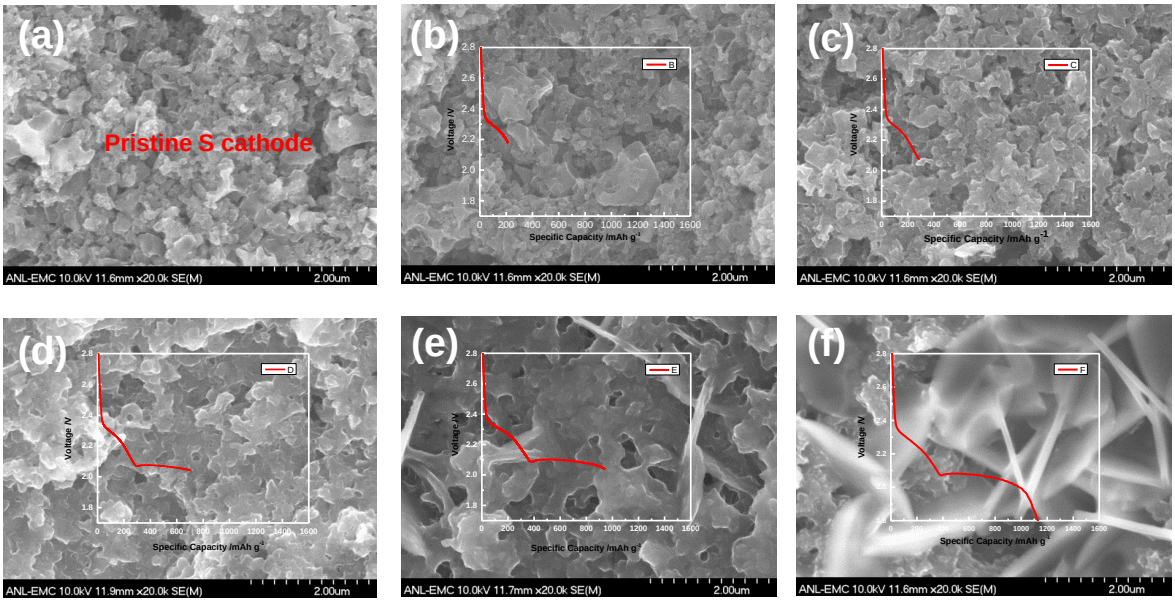

Figure 6. SEM images of sulfur electrode at (a) pristine, (b) 15% DOD, (c) 25% DOD, (d) 45% DOD, (e) 85% DOD and (f) 100% DOD with baseline electrolyte 1.0 M LiTFSI DOL/DME (5/5). (the magnification is not reflecting the real one due to the re-scaled images; Insets are the discharge voltage profiles at different DOD where the SEM measurement was taken).

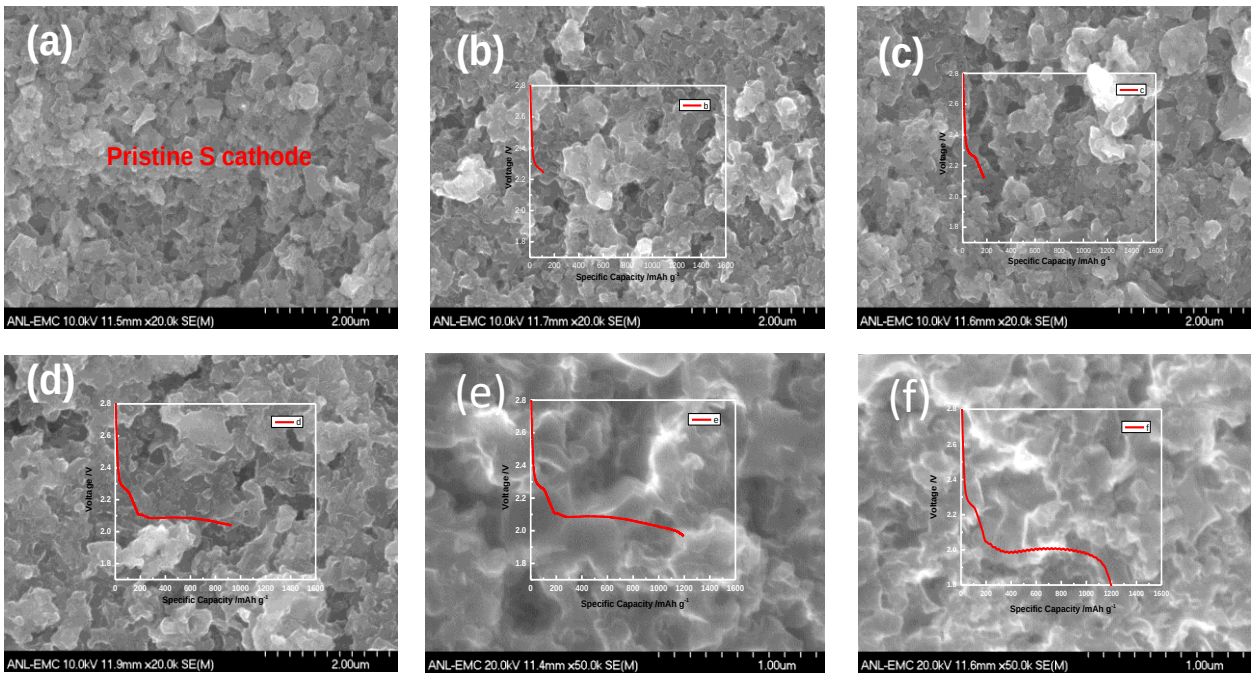

Figure 7. SEM images of sulfur electrode at (a) pristine, (b) 15% DOD, (c) 25% DOD, (d) 45% DOD, (e) 85% DOD and (f) 100% DOD with electrolyte 1.0 M LiTFSI DOL/TFEE (5/5). (the magnification is not reflecting the real one due to the re-scaled images; Insets are the discharge voltage profiles at different DOD where the SEM measurement was taken).

4. Conclusions

A high performance LiSB with FSPC coupled with DOL/TFEE based electrolyte was developed and thoroughly examined by electrochemistry and morphology methods. Due to the weak solvation with Li^+ either from the dissolved lithium salt or the discharged LiPS, the new fluorinated electrolyte has low chelating capacity with additional Li^+ resulted from all the discharged products of Li_2S_x ($2 \leq x \leq 8$). This effect intrinsically prevents the LiPS dissolution and suppresses the subsequent shuttling effect and loss of active sulfur materials during the repeated charge-discharge process. Furthermore, when coupled with FSPC, the LiSB showed fabulous cycling performance

offering an ultimate solution for mitigating the fast capacity fading of the traditional LiSB chemistry. Electrolytes in batteries must cater to the needs of both electrodes; hence, in principle, new battery chemistries would have incurred new electrolyte compositions. Future studies will focus on further tuning the structure-property relationship of the fluorinated ether and the architecture of the electrode to find the final solution for the ideal LiSB.

Author Contributions

The manuscript was written through contributions of all authors. All authors have given approval to the final version of the manuscript.

Acknowledgements

This research is supported by Daimler AG/Mercedes-Benz Research & Development North America, Inc. Argonne, a U.S. Department of Energy laboratory, is operated by UChicago Argonne, LLC under contract DE-AC02-06CH11357. SEM/EDS analysis was performed at Electron Microscopy Center at Argonne National Laboratory. The authors wish to thank the Beijing University of Chemical Technology for the International Joint Graduate -Training Program Scholarship.

References

(1) Scrosati, B.; Hassoun, J.; Sun, Y.-K. Lithium-Ion Batteries. A Look into the Future. *Energy Environ. Sci.* **2011**, *4*, 3287-3295.

(2) Ji, X.; Nazar, L. F. Advances in Li–S Batteries. *J. Mater. Chem.* **2010**, *20*, 9821-9826.

(3) Thackeray, M. M.; Wolverton, C.; Isaacs, E. D. Electrical Energy Storage for Transportation-Approaching the Limits of, and Going Beyond, Lithium-ion batteries. *Energy Environ. Sci.* **2012**, *5*, 7854-7863.

(4) Scrosati, B.; Garche, J. Lithium batteries: Status, Prospects and Future. *J. Power Sources* **2010**, *195*, 2419-2430.

(5) Wang, H.; Yang, Y.; Liang, Y.; Robinson, J. T.; Li, Y.; Jackson, A.; Cui, Y.; Dai, H. Graphene-Wrapped Sulfur Particles as a Rechargeable Lithium-Sulfur Battery Cathode Material with High Capacity and Cycling Stability. *Nano Lett.* **2011**, *11*, 2644-2647.

(6) Su, Y. S.; Fu, Y.; Cochell, T.; Manthiram, A. A Strategic Approach to Recharging Lithium-Sulphur Batteries for Long Cycle Life. *Nat. Commun.* **2013**, *4*, 2985.

(7) Chen, L.; Shaw, L. L. Recent Advances in Lithium–Sulfur Batteries. *J. Power Sources* **2014**, *267*, 770-783.

(8) Evers, S.; Nazar, L. F. New Approaches for High Energy Density Lithium-Sulfur Battery Cathodes. *Acc. Chem. Res.* **2012**, *46*, 1135-1143.

(9) Wang, L.; Byon, H. R. N-Methyl-N-propylpiperidinium Bis(trifluoromethanesulfonyl)imide-Based Organic Electrolyte for High Performance. Lithium–Sulfur Batteries. *J. Power Sources* **2013**, *236*, 207-214.

(10) Marmorstein, D.; Yu, T. H.; Striebel, K. A.; McLarnon, F. R.; Hou, J.; Cairns, E. J. Electrochemical Performance of Lithium/Sulfur Cells with Three Different Polymer Electrolytes. *J. Power Sources* **2000**, *89*, 219-226.

(11) Bruce, P. G.; Hardwick, L. J.; Abraham, K. M. Lithium-Air and Lithium-Sulfur Batteries. *MRS Bulletin* **2011**, *36*, 506-512.

(12) Hofmann, A. F.; Fronczek, D. N.; Bessler, W. G. Mechanistic Modeling of Polysulfide Shuttle and Capacity Loss in Lithium–Sulfur Batteries. *J. Power Sources* **2014**, *259*, 300-310.

(13) Zhang, S. S. Liquid Electrolyte Lithium/Sulfur Battery: Fundamental Chemistry, Problems, and Solutions. *J. Power Sources* **2013**, *231*, 153-162.

(14) Cañas, N. A.; Wolf, S.; Wagner, N.; Friedrich, K. A. In-Situ X-Ray Diffraction Studies of Lithium–Sulfur Batteries. *J. Power Sources* **2013**, *226*, 313-319.

(15) Barchasz, C.; Molton, F.; Duboc, C.; Leprêtre, J.-C.; Patoux, S.; Alloin, F. Lithium/Sulfur Cell Discharge Mechanism: An Original Approach for Intermediate Species Identification. *Anal. Chem.* **2012**, *84*, 3973-3980.

(16) Kawase, A.; Shirai, S.; Yamoto, Y.; Arakawa, R.; Takata, T. Electrochemical Reactions of Lithium–Sulfur Batteries: An Analytical Study Using the Organic Conversion Technique. *Phys. Chem. Chem. Phys.* **2014**, *16*, 9344-9350.

(17) Zhang, S. S. New Insight into Liquid Electrolyte of Rechargeable Lithium/Sulfur Battery. *Electrochim. Acta* **2013**, *97*, 226-230.

(18) Zhang, S. S.; Read, J. A. A New Direction for the Performance Improvement of Rechargeable Lithium/Sulfur Batteries. *J. Power Sources* **2012**, *200*, 77-82.

(19) Nelson, J.; Misra, S.; Yang, Y.; Jackson, A.; Liu, Y.; Wang, H.; Dai, H.; Andrews, J. C.; Cui, Y.; Toney, M. F. In Operando X-ray Diffraction and Transmission X-ray Microscopy of Lithium Sulfur Batteries. *J. Am. Chem. Soc.* **2012**, *134*, 6337-6343.

(20) Yeon, J.-T.; Jang, J.-Y.; Han, J.-G.; Cho, J.; Lee, K. T.; Choi, N.-S. Raman Spectroscopic and X-ray Diffraction Studies of Sulfur Composite Electrodes during Discharge and Charge. *J. Electrochem. Soc.* **2012**, *159*, A1308-A1314.

(21) Jeong, S.; Bresse, D.; Buchholz, D.; Winter, M.; Passerini, S. Carbon coated lithium sulfide particles for lithium battery cathodes. *J. Power Sources* **2013**, *235*, 220-225.

(22) Zu, C.; Su, Y.-S.; Fu, Y.; Manthiram, A. Improved Lithium-Sulfur Cells with a Treated Carbon Paper Interlayer. *Phys. Chem. Chem. Phys.* **2013**, *15*, 2291-2297.

(23) Gao, M. Y.; Li C. M.; Liu N.Q.; Chen Y.L.; Wang W.K.; Zhang H.; Yu Z.B.; Huang Y.Q. Inhibition on polysulfides dissolve during the discharge-charge by using fish-scale-based porous carbon for lithium-sulfur battery. *Electrochim. Acta* **2014**, *149*, 258-263.

(24) Zhao, S. R.; Li, C.M.; Wang, W.K.; Zhang, H.; Gao, M.Y.; Xiong, X.; Wang, A.B.; Yuan, K.G.; Huang, Y.Q.; Wang, F. A novel porous nanocomposite of sulfur/carbon obtained from fish scales for lithium-sulfur batteries. *J. Mater. Chem. A* **2013**, *1*(10), 3334-3339.

(25) Wei, S., Zhang, H., Huang, Y., Wang, W., Xia, Y., and Yu, Z. Pig bone derived hierarchical porous carbon and its enhanced cycling performance of lithium-sulfur batteries. *Energy Environ. Sci.* **2011**, 4(3), 736-740.

(26) Rybarczyk, M. K., Peng, H. J., Tang, C., Lieder, M., Zhang, Q., and Titirici, M. M. Porous carbon derived from rice husks as sustainable bioresources: insights into the role of micro-/mesoporous hierarchy in hosting active species for lithium-sulphur batteries. *Green Chemistry*, **2016**, *18(19)*, 5169-5179.

(27) Li, G., Sun, J., Hou, W., Jiang, S., Huang, Y., and Geng, J. Three-dimensional porous carbon composites containing high sulfur nanoparticle content for high-performance lithium-sulfur batteries. *Nat. commun.* **2016**, *7*, 10601.

(28) Chung, K.-I.; Kim, W.-S.; Choi, Y.-K. Lithium Phosphorous Oxynitride as a Passive Layer for Anodes in Lithium Secondary Batteries. *J. Electroanal. Chem.* **2004**, *566*, 263-267.

(29) Lee, Y. M.; Choi, N.-S.; Park, J. H.; Park, J.-K. Electrochemical Performance of Lithium/Sulfur Batteries with Protected Li Anodes. *J. Power Sources* **2003**, *119-121*, 964-972.

(30) Nagao, M.; Hayashi, A.; Tatsumisago, M. Electrochemical Performance of All-Solid-State Li/S Batteries with Sulfur-Based Composite Electrodes Prepared by Mechanical Milling at High Temperature. *Energy Technol.* **2013**, *1*, 186-192.

(31) Hassoun, J.; Scrosati, B. Moving to a Solid-State Configuration: A Valid Approach to Making Lithium-Sulfur Batteries Viable for Practical Applications. *Adv. Mater.* **2010**, *22*, 5198-5201.

(32) Yuan, L. X.; Feng, J. K.; Ai, X. P.; Cao, Y. L.; Chen, S. L.; Yang, H. X. Improved Dischargeability and Reversibility of Sulfur Cathode in a Novel Ionic Liquid Electrolyte. *Electrochem. Commun.* **2006**, *8*, 610-614.

(33) Shin, J.H.; Cairns, E.J. N-Methyl-(n-butyl) pyrrolidinium Bis(trifluoromethanesulfonyl) imide-LiTFSI Poly(ethylene glycol) dimethyl Ether Mixture as a Li/S Cell Electrolyte. *J. Power Sources* **2008**, *177*, 537-545.

(34) Dokko, K.; Tachikawa, N.; Yamauchi, K.; Tsuchiya, M.; Yamazaki, A.; Takashima, E.; Park, J.-W.; Ueno, K.; Seki, S.; Serizawa, N.; Watanabe, M. Solvate Ionic Liquid Electrolyte for Li–S Batteries. *J. Electrochem. Soc.* **2013**, *160*, A1304-A1310.

(35) Ryu, H.-S.; Ahn, H.-J.; Kim, K.-W.; Ahn, J.-H.; Cho, K. K.; Nam, T.-H.; Kim, J.-U.; Cho, G.-B. Discharge Behavior of Lithium/Sulfur Cell with TEGDME Based Electrolyte at Low Temperature. *J. Power Sources* **2006**, *163*, 201-206.

(36) Chang, D.-R.; Lee, S.-H.; Kim, S.-W.; Kim, H.-T. Binary Electrolyte Based on Tetra(ethylene glycol) Dimethyl Ether and 1,3-Dioxolane for Lithium–Sulfur Battery. *J. Power Sources* **2002**, *112*, 452-460.

(37) Aihara, Y.; Bando, T.; Nakagawa, H.; Yoshida, H.; Hayamizu, K.; Akiba, E.; Price, W. S. Ion Transport Properties of Six Lithium Salts Dissolved in γ-Butyrolactone Studied by Self-Diffusion and Ionic Conductivity Measurements. *J. Electrochem. Soc.* **2004**, *151*, A119-A122.

(38) Lin, Z.; Liu, Z.; Fu, W.; Dudney, N. J.; Liang, C. Phosphorous Pentasulfide as a Novel Additive for High-Performance Lithium-Sulfur Batteries. *Adv. Funct. Mater.* **2013**, *23*, 1064-1069.

(39) Liang, C.; Dudney, N. J.; Howe, J. US DOE-EERE Vehicle Technologies Office Program Annual Merit Review and Peer Evaluation Meeting, Washington D.C., May **2011**.

(40) Azimi, N.; Weng, W.; Takoudis, C.; Zhang, Z. Improved Performance of Lithium–Sulfur Battery with fluorinated electrolyte. *Electrochem. Commun.* **2013**, *37*, 96-99.

(41) Cuisinier, M., Cabelguen, P. E., Adams, B. D., Garsuch, A., Balasubramanian, M., and Nazar, L. F. Unique behaviour of nonsolvents for polysulphides in lithium-sulphur batteries. *Energy Environ. Sci.* **2014**, *7(8)*, 2697-2705.

(42) Lu, H., Yuan, Y., Zhang, K., Qin, F., Lai, Y., and Liu, Y. Application of partially fluorinated ether for improving performance of lithium/sulfur batteries. *J. Electrochem. Soc.* **2015**, *162(8)*, A1460-A1465.

(43) Zu, C., Azimi, N., Zhang, Z., and Manthiram, A. Insight into lithium-metal anodes in lithium-sulfur batteries with a fluorinated ether electrolyte. *J. Mater. Chem. A* **2015**, *3(28)*, 14864-14870.

(44) Azimi, N., Xue, Z., Bloom, I., Gordin, M. L., Wang, D., Daniel, T., Takoudis, C. and Zhang, Z. Understanding the Effect of a Fluorinated Ether on the Performance of Lithium-Sulfur Batteries. *ACS App. Mater. Interfaces* **2015**, *7(17)*, 9169-9177.

(45) Gordin, M. L., Dai, F., Chen, S., Xu, T., Song, J., Tang, D., Azimi, N., Zhang, Z. and Wang, D. Bis (2, 2, 2-trifluoroethyl) Ether As an Electrolyte Co-solvent for Mitigating Self-Discharge in Lithium–Sulfur Batteries. *ACS Appl. Mater. Interfaces* **2014**, *6(11)*, 8006-8010.

(46) Cheng, L., Curtiss, L.A., Zavadil, K.R., Gewirth, A.A., Shao, Y., and Gallagher, K. G. Sparingly Solvating Electrolytes for High Energy Density Lithium-Sulfur Batteries. *ACS Energy Lett.* **2016**, *1*, 503-509.

Supplemental Information

A High Performance Lithium-Sulfur Battery Enabled by Fish-Scale Porous Carbon/Sulfur Composite and Symmetric Fluorinated Diethoxyethane Electrolyte

Mengyao Gao[a, d], ChiCheung Su[a], Meinan He[a], Tobias Glossmann[b], Andreas Hintennach[c], Zhenxing Feng[a], Yaqin Huang[d], Zhengcheng Zhang[a,*]

Email: zzhang@anl.gov, 1-630-252-7868

1. NMR Spectroscopy Characterization of TFEE

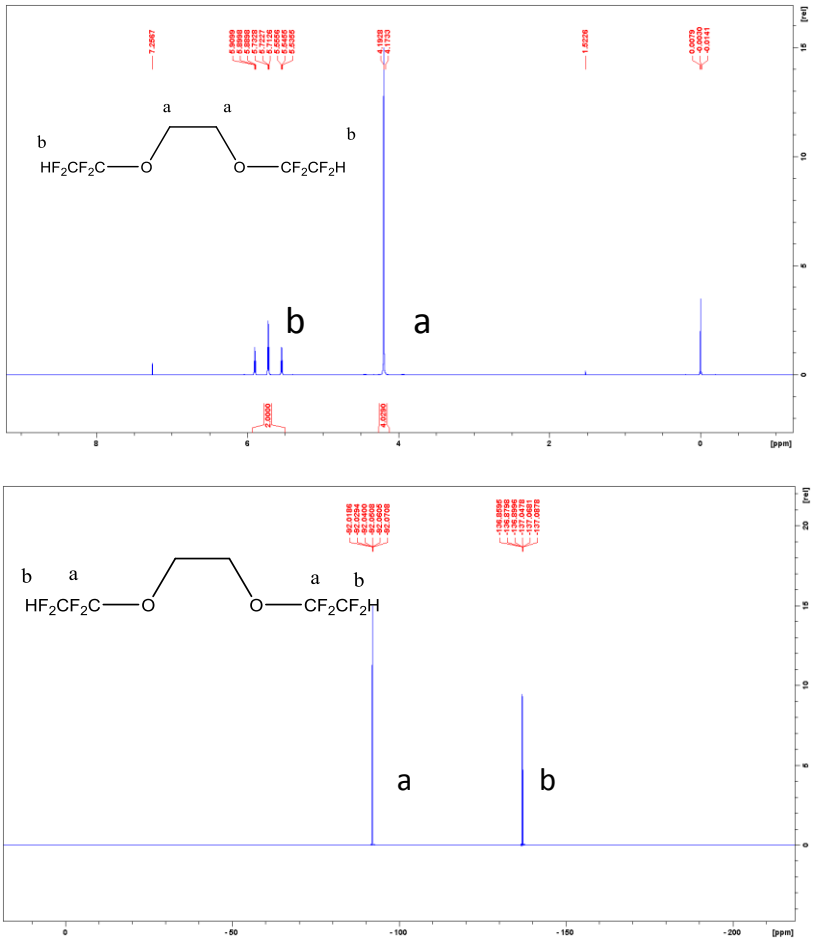

Figure S1. ^{1}H (top) and ^{19}F-NMR (bottom) spectra of 1,2-bis(1,1,2,2-tetrafluoroethoxy) ethane.

2. Cyclic Voltammograms of Li-S Cells with Fluorinated and Baseline Electrolytes

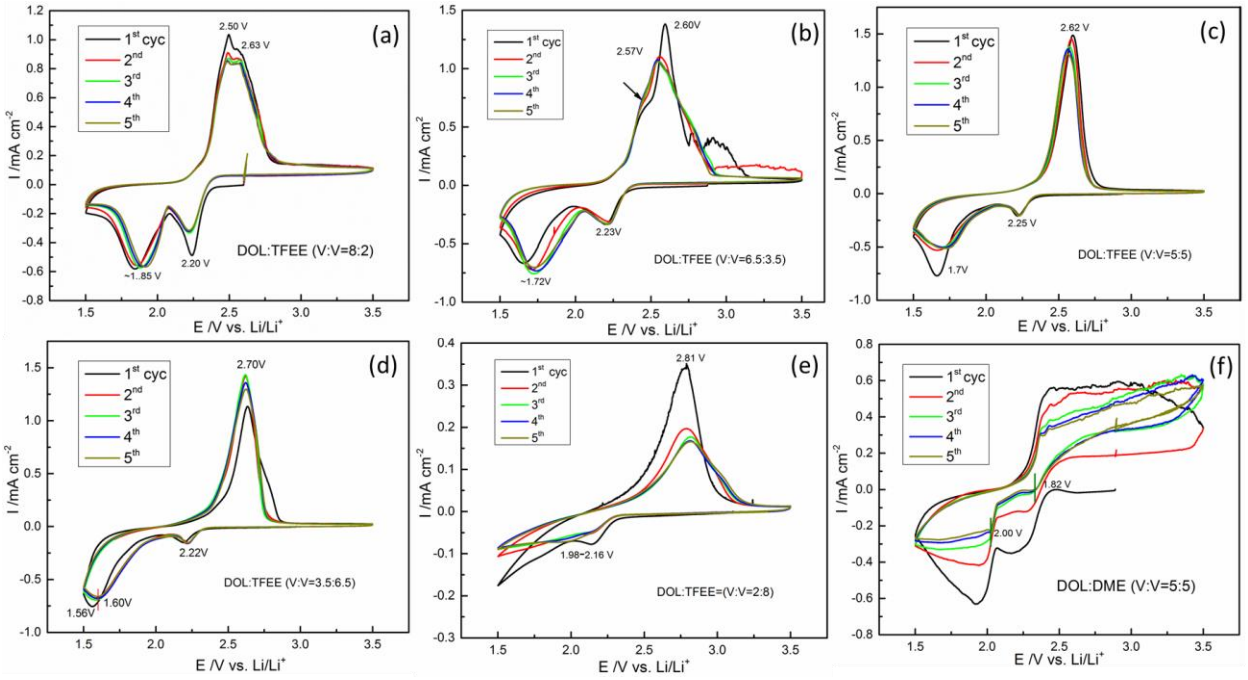

Figure S2. Cyclic voltammetry of the Li-S cells with electrolyte (a) 1.0 M LiTFSI DOL/TFEE (8/2), (b) 7/3, (c) 5/5, (d) 4/6, (e) 2/8, and (f) baseline 1.0 M LiTFSI DOL/DME (5/5) electrolyte. (All ratios are volumetric rations).

3. Lithium Polysulfides Dissolution in Electrolytes

Coin cells were disassembled in the first discharge cycle at various depth of discharge (DOD) 15%, 25%, 45%, 85% and 100%. The coin cell parts (electrodes, separator and stainless spacers) were rinsed by 10 mL DME solvent to harvest the electrolyte.

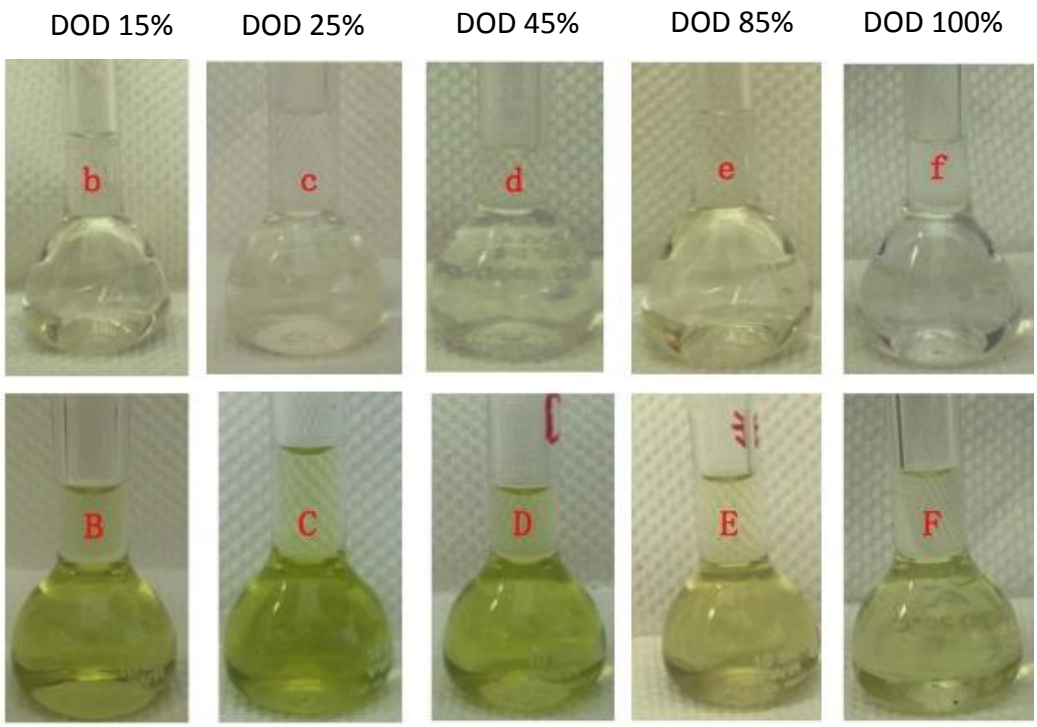

Figure S3. Harvested electrolyte from coin cells at DOD stage of 15%, 25%, 45%, 85% and 100% diluted with DOL solvent. Top figures from b to f: 1.0 M LiTFSI DOL/TFEE (5/5) electrolyte; Bottom figures from B to F: 1.0 M LiTFSI DOL/DME (5/5) electrolyte.

4. SEM/EDS of the Fish-Scale Porous Carbon/Sulfur Cathode

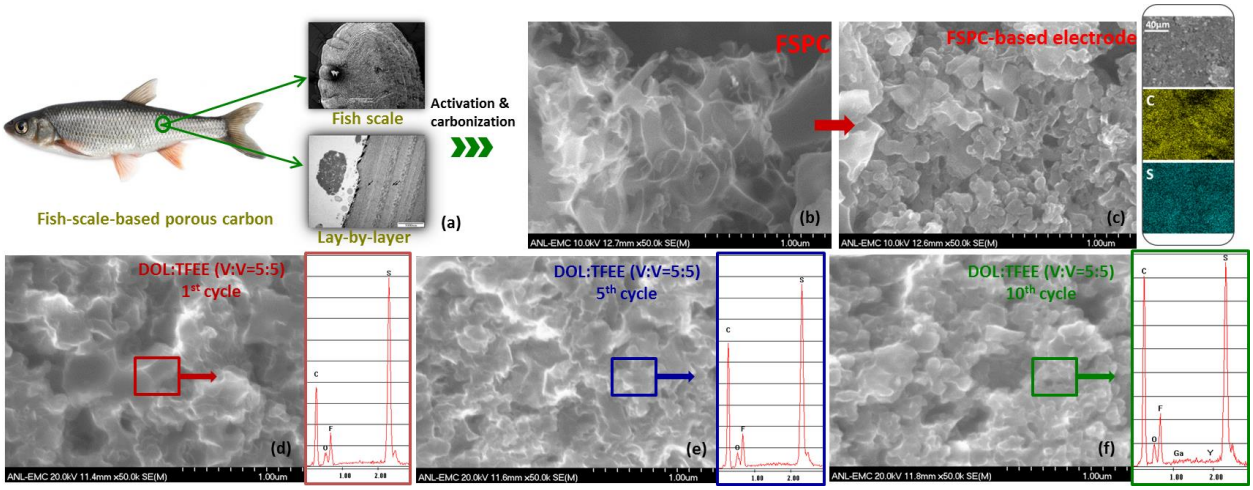

Figure S4. (a) Fish-scale porous carbon (FSPC) fabrication process and SEM image of (b) FSPC,

(c) FSPC/sulfur composite electrode, (d) electrode after 1st cycle, (e) after 5th cycle, and (f) after 10th cycle with 1.0 M LiTFSI DOL/TFEE (5/5) electrolyte. C and S elemental mapping is shown adjacent to (c), EDS spectra for electrode after 1st, 5th and 10th were shown adjacent to (d), (e) and (f), respectively.

5. Sulfur Electrode Morphology after 100 Cycles

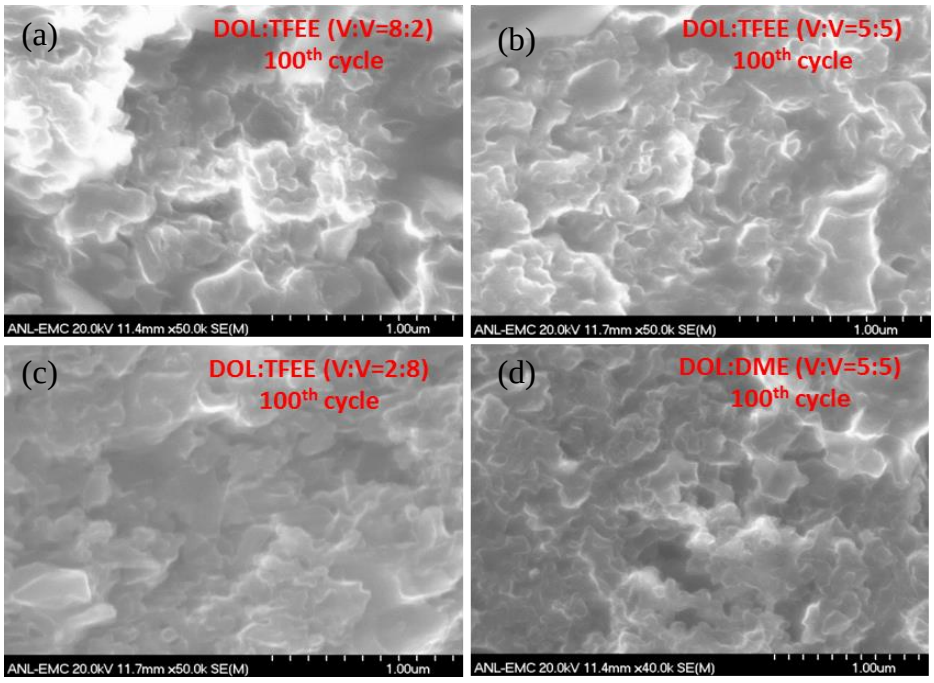

Figure S5. SEM image of FSPC/sulfur electrode after 100 cycles in different electrolytes. (a) 1.0 M LiTFSI DOL/TFEE (8/2), (b) 1.0 M LiTFSI DOL/TFEE (5/5), (c) 1.0 M LiTFSI DOL/TFEE (2/8), and (d) 1.0 M LiTFSI DOL/DME (5/5).

Table S1. Fitted values for the equivalent circuit by simulation of impedance spectra

Stage	$R_1(\Omega)$	R_2 (Ω)	CPE1
OCV	14.32	146.60	8.3595E-6
a	14.95	140.30	8.1405E-6
b	16.30	90.36	8.3621E-6
c	17.85	140.00	6.5119E-5
d	19.19	100.20	1.3384E-5
e	17.76	82.81	1.4332E-5
f	18.33	97.38	1.2624E-5
g	17.36	63.65	1.4324E-5
h	17.51	99.52	1.5147E-5